

Nanostructured ZnO as Biomimetic Anti-reflective Coatings on Textured Silicon Using a Continuous Solution Process

Seung-Yeol Han,^{a,*} Brian K. Paul^b and Chih-hung Chang^{a,*}

^a *School of Chemical, Biological, and Environmental Engineering, Oregon State University, 102
Gleeson Hall Corvallis, OR, 97331, USA.*

^b *School of Mechanical, Industrial and Manufacturing Engineering, Oregon State University,
204 Rogers Hall, Corvallis, OR, 97331, USA.*

** To whom correspondence should be addressed.*

Email: hanse@engr.orst.edu, changch@engr.orst.edu

Abstract

A novel table-top, microreactor-assisted nanomaterial deposition (MANDTM) process, which combines the merits of microreaction technology with solution-phase nanomaterial synthesis and film deposition, was used to grow a nanostructured ZnO anti-reflective coating on a textured silicon substrate from aqueous solution. The subwavelength, anti-reflective nanostructures mimicked the structure and performance of the surface of the eye from a night-flying moth. Solution-processed Ag nanoparticles were applied as a seed layer on the textured silicon surface leading to preferred heterogeneous nucleation and good area coverage. Preferential growth of the nanostructured ZnO was controlled by changing residence time, reaction temperature, and concentration of precursor solution without the use of a buffer reagent (e.g. HMTA). Well-aligned ZnO nanorod arrays were fabricated by MAND at a very high deposition rate (i.e 125 nm/min) compared to batch hydrothermal method. The surface reflection of the polished silicon was suppressed from an average of 30.8% between wavelengths of 400 and 900 nm to 10.6% after micro-scale pyramidal surface texturing to 3.4% after application of the ZnO nanostructure on the textured silicon. The results provide a potential economical path to broadband anti-reflection (AR) for silicon wafers and solar cell substrates.

1. Introduction

The increased availability of nano-scale materials and structures has enabled technology pioneers to address many performance challenges across a vast range of applications. One approach to application development has been to emulate nanostructures discovered in nature. For example, researchers have found ways to mimic a gecko's toe for medical adhesives and climbing robots, a butterfly's wing for display surfaces, the Namib desert beetle's back and a lotus leaf for harvesting water in dry regions, and a moth's eye for antireflective coating.¹⁻⁴

A great deal of recent research has focused on using nanostructured thin films for highly efficient light energy conversion. One area for enhancing light conversion efficiency is to minimize the loss of light transmission due to reflection at optical interfaces. Loss of light through reflection severely impacts the performance of various optical and optoelectronic components such as eyeglasses,⁵ solar cells,⁶ and flat panel displays⁷. One way to combat this issue is to apply an anti-reflective coating on the surface with the goal to reduce or eliminate the reflected light. Without the anti-reflective coatings, reflected light can cause glare on a display or a screen. The reflected light could also cause window or windshield glare which could impair the vision of a driver.

A graded index of refraction at the interface between two media has been found to significantly reduce light reflection at the interface. Recent, state-of-the-art advances report a seven-layer vapor-deposited film which reduced the surface reflectance of a silicon surface to a wavelength-averaged total reflectance of 3.79% between 400 and 2000 nm.⁸ The requirement of multiple vacuum-processed steps leads to a lower throughput and higher capital cost that is not ideal for low-cost, large area applications.

The eyes of night-flying moths found in nature have demonstrated a broadband anti-reflective property. This line of work extends from an investigation by Bernhard in 1967 to determine the means by which night-flying moths camouflage eye reflections.⁹ Using scanning electron microscopy, Bernhard discovered a periodic array of sub-wavelength protrusions on the cornea of the moths. It was found that these so-called “moth-eye” structures work on the principle of a gradient index of refraction. Because the features on a moth-eye surface are below the wavelength of light to be transmitted, incident light cannot resolve them. Consequently, these surfaces act as a metamaterial possessing surface properties as a weighted average of the two media. These gradient surfaces are thought to have a low net reflectance based on the destructive interference of an infinite series of reflections at each incremental change in refractive index.

For these reasons, numerous nanostructured films have been fabricated to mimic the moth-eye structure. Various approaches to produce subwavelength-structured AR surfaces as efficient broadband AR layers have been investigated including porous, periodic surface relief and stochastic surface-relief structures.^{10,11} Various nanostructured film fabrication technologies have been employed such as electron-beam evaporation,¹² chemical vapor deposition (CVD),¹³⁻¹⁵ rf sputtering,¹⁶ plasma etching,¹⁷ reactive ion etching (RIE),¹⁸⁻²¹ thermal evaporation, nanoimprinting,^{22,23} sol-gel,²⁴ hydrothermal^{25,26} and chemical bath deposition (CBD).²⁷ Min *et al.* and Li *et al.* fabricated excellent moth-eye structures with an extremely low reflectance (< 2.5% on silicon and < 0.5% on glass) using the RIE technique.^{19,20} Nakanishi *et al.* fabricated a moth-eye structure with a much reduced reflection (< 0.8%) on silicon using a combination of RIE and nanoimprinting.²¹ However, these processes require multiple steps including expensive lithography and vacuum processing units which are not ideal for low cost, large area, and high throughput applications. Chao *et al.* synthesized ZnO nanorod arrays (NRAs) for light scattering

by nanostructured AR coatings *via* hydrothermal growth. ZnO NRAs were well-aligned with excellent AR property. However, the process requires long reaction times (hours).²⁵

We have developed microreactor-assisted nanomaterial deposition (MANDTM) (scheme 1) as a potentially cost effective and environmentally green approach to solution processing. MANDTM combines the merits of microreaction technology with solution-phase nanomaterial synthesis and film deposition. The large surface-area-to-volume ratios in microchannel reactors afford accelerated and tightly controlled heat and mass transport leading to more uniform heating and mixing. This process takes advantage of microreaction technology and the large library of near room temperature, liquid-phase nanomaterial synthesis recipes to produce and assemble nanofilms at the point-of-deposition. It is expected that this process will be more easily scalable than conventional solution-based processes offering the possibility to minimize the environmental impact of nanomanufacturing practices through solvent-free mixing and integrated separation. Point-of-use synthesis has the potential to eliminate the need to store and transport hazardous nanomaterials.

For these reasons, MANDTM has been pursued in many solution processing applications.²⁸⁻³⁵

Deposition has been performed by many methods, such as spinning disk, flow cell, spray deposition, aerosol, or reel-to-reel coating. Our group has been actively investigating the synthesis of nanoparticles and thin film deposition by MANDTM.^{36,37}

Nanostructured ZnO has been widely used as an attractive material in solar cell applications due to its high optical transparency, low cost, appropriate refractive index ($n = 2.0$) and versatility to form different nanostructures.^{14,15,23,25-27,38} There are limited reports in the literature regarding growing nanostructured ZnO on a textured pyramidal Si surface.^{14,26} In this study, biomimetic nanostructured ZnO films were produced at high deposition rate using

a low-temperature MANDTM process, exhibiting excellent anti-reflection on textured pyramidal silicon surfaces. The morphology of ZnO nanostructured thin film is also tunable by controlling the process parameters.

2. Experimental

2.1 Preparation of textured pyramidal silicon substrate

Polished silicon (100) wafers were used as substrates. The silicon substrate was rinsed with detergent and dried by flowing nitrogen gas. To create the textured surface, the silicon substrate was emerged into 2 vol. % of isopropyl alcohol (IPA) in 0.5 M sodium hydroxide (NaOH, Mallinckrodt Chemicals) at 80 °C for 30 minutes. The etching solution was stirred at 400 rpm in order to achieve consistent etching quality. The textured pyramidal surface of silicon substrate was then rinsed with DI water, diluted HCl, and DI water again. Finally, it was dried by a stream of dry nitrogen gas.

2.2 Preparation of Ag nanoparticles

Ethylene glycol (EG, HO(CH₂)₂OH, Mallinckrodt Chemicals), polyvinylpyrrolidone (PVP, (C₆H₉NO)_n, MW 40,000, Alfa Aesar), and silver nitrate (AgNO₃, ACS 99.9+%, Alfa Aesar) were purchased and used without further purification. In synthesis, 3 g of PVP was added into 75 ml of EG under magnetic stirring in a 50 mL beaker maintained at 120°C. After the PVP was completely dissolved, 0.4g of AgNO₃ was added. Ag NPs were synthesized at 120°C for 2 h. The solution was left to cool at room temperature. The peaks of XRD obtained from Ag NPs on a glass slide substrate correspond to the (1 1 1), (2 0 0), (2 2 0), and (3 1 1) planes of face-centered cubic (fcc). Ag NPs were deposited on the textured pyramidal surface of the silicon substrate by spin coating at 2000 rpm.

2.3 Deposition of nanostructured ZnO on textured surface

Two stock solutions were prepared. 200 ml aqueous solution of 5 mM zinc acetate ($\text{Zn}(\text{COOCH}_3)_2 \cdot 2\text{H}_2\text{O}$, Sigma Aldrich) and 10 ml aqueous solution of 0.25 M ammonium acetate ($\text{CH}_3\text{COONH}_4$, Mallinckrodt Chemicals) were well mixed and prepared as solution I. Solution II was composed of 200 ml aqueous solution of 0.1 M sodium hydroxide (NaOH, Mallinckrodt Chemicals). The two stock solutions, containing reactive species, were pumped by a compact REGLO peristaltic tubing pump (ISMATEC) and mixed through a T-mixer (P-727, Upchurch Tee Peek, 1/16 in. 0.02 thru hole). The mixed solution was passed through 1.22 mm ID Tygon tubing along 1 m length which was maintained at 70 °C by water circulation with a residence time of 6.2 sec after the mixing.

The resulting mixture was impinged on the surface of textured silicon. The substrate was placed on a rotating substrate holder maintained at a constant temperature of 70 °C, controlled by a heating coil and thermocouple. First, the seed layer of Ag nanoparticles were deposited on the textured surface of the silicon substrate. Next, the substrate was spun at 2400 rpm for a few seconds and then the mixture of reactive solution was impinged on top of the Ag seed layer. The rotating speed for the deposition of nanostructured ZnO on the textured silicon was reduced and kept at 300 rpm. The deposition time for the highly dense and crystalline nanostructured ZnO was 4 min. Finally, the as-deposited nanostructured ZnO was dried on a hot plate at 100 °C for a few minutes to evaporate water and any remaining solvents.

2.4 Characterization

Scanning electron microscopy (SEM, FEI Quantum 600 FEG) was employed for cross sectional analysis and surface morphology characterization. Integrated sphere reflection measurement

(Ocean Optics Inc, USB HR 2000+, ISP-30-6-R integrating sphere) were employed to measure the reflectance of surfaces. X-ray diffraction (XRD, Bruker D8 discover) was conducted to determine the phase and crystalline orientation of the nanostructured ZnO.

3. Results and discussion

The growth of well-aligned ZnO nanorods on the Ag nanoparticle seeded surface was achieved in aqueous solution by promoting the heterogeneous nucleation on the surface of the Ag nanoparticles, and by controlling the degree of supersaturation by the MANDTM process.

3.1 Effect of heterogenous nucleation

In a batch CBD process, both heterogeneous and homogeneous reactions occur in the solution. Homogeneous nucleation in the solution results in the formation of nanoparticles that would deposit and serve as a seed for the growth of random-aligned ZnO film. The flower-like nanostructured ZnO film shown in figure 1 is an example. Figure 1a & b show the top view and tilted cross sectional image of the textured silicon. Figure 1c ~ f show different coverage of the nanostructured ZnO deposition on the textured silicon surface. A mixture of ZnO precursor solution from the microreactor was delivered to the textured surface for 4 minutes. Nanostructured ZnO mainly grew in the valleys of the textured surface because the reacting solution mixture has more contact time in the valleys of the textured surface. It is likely that the ZnO nuclei were formed homogeneously then served as a seed to facilitate the continuous growth of ZnO on the textured surface. This resulted in a ZnO nanostructure that covered less than 50 % of the textured silicon surface.

An illustration of the growth of flower-like nanostructures is shown in figure 2d. The SEM image given in figure 1e shows ZnO nanostructures grown on textured Si after being treated with

a precursor solution of zinc acetate and ammonium acetate. This treatment was employed as a source of a seed layer for enhancing coverage and growth rate of ZnO nanostructures. It can be seen clearly by comparing the SEM images that a higher coverage of ZnO was obtained on the textured silicon with the zinc precursor seed layer treatment. The coverage of nanostructured ZnO deposition on the zinc precursor seed layer was about 50~70 % and is presented in Figure 1e & f. This is higher than the deposition without any pretreatment. It is likely that the zinc precursor film provides nucleation sites to facilitate the subsequent nanostructured ZnO growth.

The surface roughness of the zinc precursor film also affects the growth of the ZnO nanostructure by providing more surface for nucleation.^{39,40} However, even with the pretreatment, voids are still present at the summit of the pyramid. The flower-like, random-aligned ZnO nanostructures were again formed on the pretreated textured silicon surface.

Random-aligned ZnO growth is likely a result of amorphous seed layer that was fabricated at low temperature from the zinc acetate precursors. The zinc acetate precursor film was not completely converted to crystalline ZnO at this low processing temperature. Formation of more orderly aligned ZnO nanostructures could be achieved if the zinc precursor film was annealed at a higher temperature to create a crystalline ZnO seed layer. However, high temperature processing is problematic and should be avoided.

3.2 Effect of Ag seed layer on ZnO nanostructure growth

In the vapor-liquid-solid (VLS) and vapor-solid (VS) nanowire growth, metallic nanomaterials such as Au and Ag nanoparticles are often used as catalysts.⁴¹⁻⁴³ Both VLS and VS nanowire growth require gas phase reactions at high processing temperature.

In this study, Ag nanoparticles prepared by a solution-based process were used as seeds for the growth of ZnO. The sizes of the Ag NPs in dispersion range approximately from 5 to 50 nm. The solution containing Ag NPs was dispensed on a rotating substrate at 2400 rpm for a few seconds. Figure 2a and 2b show the textured surface of silicon substrate with and without Ag NPs, respectively. Ag NPs can be seen uniformly deposited on the entire textured surface from figure 2c. After the deposition of Ag NPs, a mixture of ZnO reacting solution was delivered to the Ag NPs seeded surface.

ZnO deposition using MAND were performed for 4 minutes. The as-deposited films were dried on a hot plate which was held at 100 °C. Figure 2e and g show two different ZnO structures on the textured silicon substrates with and without Ag NPs seeds, respectively. SEM images of flower-like ZnO structures on bare textured Si substrate (i.e. without Ag seeds) are shown in figure 2d and 2e. In contrast, figure 2f and 2g show well-aligned ZnO nanorods on textured silicon substrate with Ag seeds. The flower-like ZnO nanostructures were likely grown from aggregated ZnO nanoparticles generated from homogeneous reaction. The growth of ZnO nanorods on Ag nanoparticles (NPs) does not follow the VLS mechanism since the growth was performed at a low temperature, below 100 °C.^{44,45} The Ag NPs lower the net interfacial energy required for the nucleation of ZnO and promote the growth of well-aligned ZnO nanorods. The corresponding growth mechanism for the formation of these two different ZnO structures is illustrated in figure 2d and f, respectively. The Ag NPs on the surface changed the surface roughness and interfacial energy of the textured surface.

3.3 Effect of degree of supersaturation on ZnO nanostructure growth

Growth of well-aligned ZnO nanorods on the surface of the Ag NP seeds was performed via an MAND process. The key to develop a solution-based process for the fabrication of well-

controlled nanostructures is an understanding of the factors that control crystal nucleation and growth in the solution. Nucleation in a typical batch process is normally occurred throughout the solution in addition to the surface of substrate. Both heterogeneous nucleation and homogeneous nucleation are present simultaneously. Therefore, film growth and particle aggregation with clustered NPs and large precipitation could be observed even on non-targeted surfaces such as reactor walls.

For well-controlled growth, reaction condition in the solution must be carefully controlled. B.C. Bunker *et al.* pointed out that control of supersaturation can be a problem, especially for systems showing extreme pH sensitivity.⁴⁶ The consumption of reagents during growth can change the levels of supersaturation and must be compensated for to achieve optimum growth conditions. Proper control over the level of supersaturation promotes film growth via heterogeneous nucleation without homogeneous precipitation. In a batch process, the consumption of reagent and the growth mechanism can change the degree of supersaturation. As a result in a batch process, well-aligned nanostructures are difficult to achieve because the solubility of the precursors and the degree of supersaturation are hard to control due to the dominating precipitation. Therefore, most solution synthesis in a batch process is carried out with the aid of complexing agents⁴⁷ or a buffer reaction in order to slow down the precipitation by homogeneous nucleation. The most commonly used $\text{Zn}(\text{NO}_3)_2$ -Hexamethyleneteramine (HMTA) chemistry is a perfect example. It was shown recently that the role of HMTA is to control the saturation index of ZnO.⁴⁸ Complex hierarchical ZnO crystals were fabricated via secondary nucleation of ZnO branches controlled by diaminoalkane molecules.⁴⁷ Another successful approach is to create a surface that promotes the heterogeneous nucleation. A seed layer formed before for during the deposition is often used to achieve this objective.⁴⁹⁻⁵¹

We were able to deliver well-controlled concentration of the precursors and degree of supersaturation simultaneously to the desired surface via the microreactor system in a MAND process. Thus, homogeneous nucleation with precipitation is significantly suppressed in a MAND process. Continuous well-controlled nucleation is induced to the functionalized surface, which initiated nucleation and enhanced the heterogeneous reaction. Therefore, high growth rate of well-aligned ZnO nanostructures could be achieved easily by MAND. The batch hydrothermal process, the most common solution-based process for the fabrication of well-aligned ZnO nanorods, normally requires a long reaction time (i.e. hours).⁵² In contrast, well-aligned ZnO nanorods with 500 nm length shown in figure 3 could be fabricated with a rather short deposition time of 4 minutes. This deposition rate is much faster than previously reported ZnO nanowire growth via both gas-phase and solution-based processes.

3.4 Mimic the moth-eye using ZnO rod arrays

Densely packed nanostructured ZnO that mimics the moth-eye could be fabricated using proper residence time, reaction temperature, and concentration of precursor solution in a MAND process. The morphology of nanostructured ZnO thin film was characterized by Scanning Electron Microscope (SEM). The mechanism of light trapping and moth-eye effect for the reduction of reflection on nanostructured surface is illustrated in figure 4a. Light trapping is achieved via the textured surface by changing the angle between the incident light and the surface. A textured pyramidal surface reduces reflection by creating a longer incident light path length through bouncing on the textured surface and introducing a gradient refractive index between the air and the surface. The well-aligned ZnO nanorod arrays on the textured silicon show a similar morphology to the corneal nipple arrays of moth-eye, which can also dramatically suppress reflection in nature.⁵³ The deposition of nanostructured ZnO was also conducted on flat

glass substrate and nanostructured ZnO actually enhances transmission shown in figure S1. Moth eye is a very good AR example from nature, but the length scale is roughly $\frac{1}{4}$ wavelength of the light. In general, AR coating is not aimed to reduce reflectance only but to enhance transmission. A large scale in feature is usually less desirable.

The reflectance measurements for bare polished, textured and nanostructured ZnO growth surface on textured silicon substrate were conducted in the UV-Vis spectrum using an integrating sphere shown in figure 4b. The average reflectance was measured within the wavelength range of 400 to 900 nm. The reflectance of textured silicon was reduced from 30.8 % of polished silicon to 10.6 %. The reflectance of ZnO nanorods on pyramidal textured surface of silicon substrate shows a significant reduction from 10.6% to 3.4% as shown in figure 4b. The averaged reflectance in the wavelength range of 400 ~ 900 nm over the AM1.5 solar photon spectral distribution with SEM images was shown at figure S2. Recently, Y. Liu et al. reports a similar approach of using ZnO nanowires growth with micropyramid silicon for antireflection coating with a low reflectance of 3.2%.²⁶ The addition of ZnO nanowires shows a significant reduction in reflection. However, the process requires the deposition of a ZnO seed layer by magnetron sputtering, a vacuum-based technique. In addition, the batch HMTA-based ZnO nanowire growth will face the difficulty in its slow growth rate.

Figure 4c shows optical images of polished silicon, textured surface silicon, random-aligned ZnO and well-aligned ZnO nanorod arrays on textured silicon surface with/without illumination. The darkest surface is obtained from surface with well-aligned ZnO nanorod arrays which indicates the light can be effectively absorbed with suppressing reflection. Suppressed reflection was clearly visualized under a strong illumination.

The crystal structure of as-deposited nanostructured ZnO was characterized by XRD. The results are shown in figure 5 with peaks at 2θ value of 31.43, 34.04, 35.93, 47.18 and 56.14 which correspond with the (100), (002), (101), (102) and (110) peaks of the hexagonal ZnO structure, respectively. All films reported in this work are as-deposited ZnO nanostructure without any post thermal treatment. The as-deposited ZnO nanostructure prepared by the MAND process exhibits polycrystalline characteristics even though the process was conducted at 70 °C.

4. Conclusions

In summary, well-aligned ZnO nanorod arrays were successfully fabricated on a textured silicon surface. The ZnO nanorod arrays were deposited on Ag NP seeds using Microreactor-Assisted Nanoparticle Deposition (MAND) process. The ZnO nanorod arrays on the textured surface are well aligned, nearly perpendicular to the silicon surface, and show a high density. The dense nanorod arrays significantly reduced the reflectance of the textured silicon surface down to 3.4%. The MAND process offered precise control over the level of supersaturation and the ability to deliver a constant flux of reactant solutions continuously. These features result in a rather fast growth rate (500 nm in 4 minutes) in contrast to previously reported ZnO nanowire growth (e.g. hours). This increase in manufacturing throughput is particularly important for solar cells.

The MAND process offers a more uniform and better controlled surface morphology along with lower cost and green, environmentally friendly processing than other ZnO nanowire growth processes like batch hydrothermal method or vapor transport processes. High crystalline nanostructured ZnO growth was achieved by MAND at a low process temperature of 70 °C and all growth processes in this study were conducted in an aqueous solution.

Acknowledgements

This work is supported by the National Science Foundation's Process and Reaction Engineering program under grant # CBET-0654434.

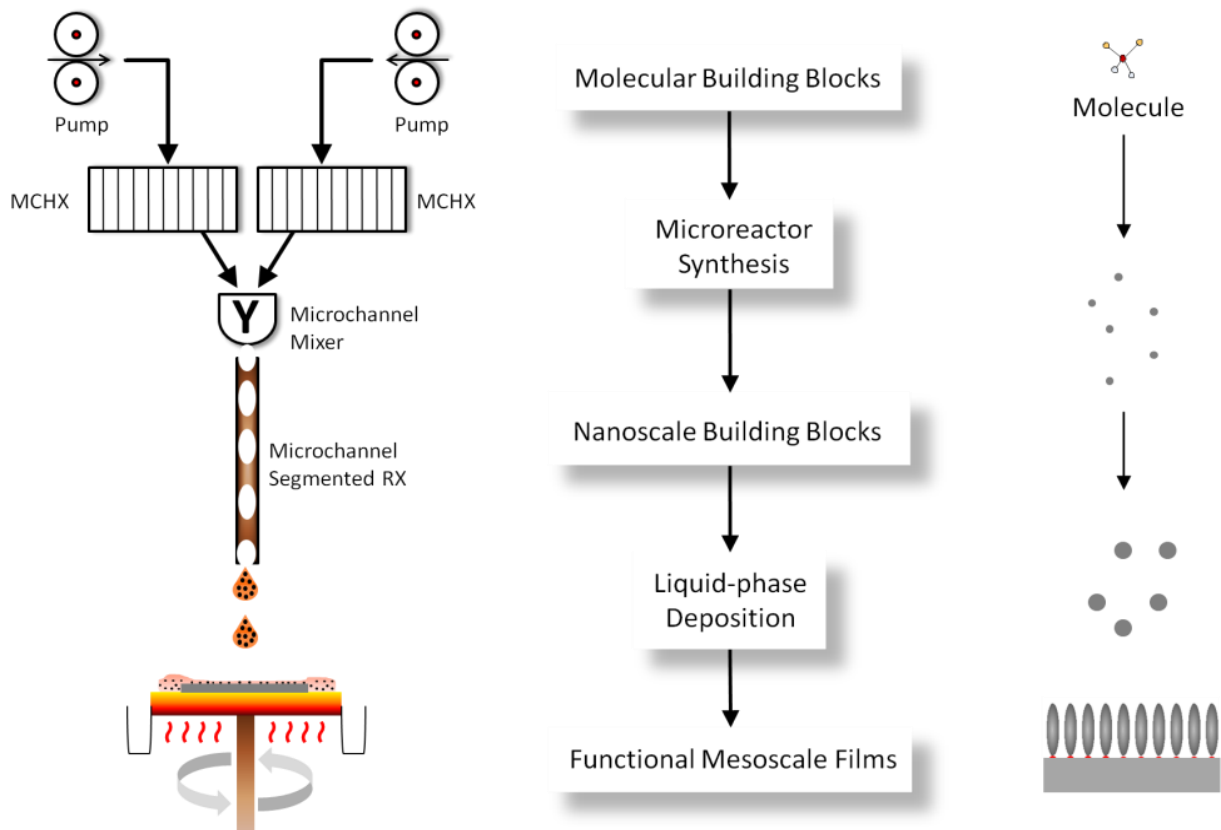
References

1. Y. Tian, N. Pesika, H. Zeng, K. Rosenberg, B. Zhao, P. McGuiggan, K. Autumn, and J. Israelachvili, *Proc. Nat. Acad. Sci.s*, 2006, 103(51),19320.
2. Z. Vértesy, Zs. Bálint, K. Kertész, J. P. vigneron, V. Lousse & L. P. Biró, *Journal of Microscopy*, 2006, 224, 108.
3. Challa S. S. R. Kumar, *Nanostructured Thin Films and Surfaces*, Wiley-VCH, 2010
4. E. Stratakis, A. Ranella, and C. Fotakis, *Biomicrofluidics*, 2011, 5, 013411.
5. H. G. Floch and P. F. Belleville, *J. Sol-Gel Sci. Tech.* 1994, 1(3), 293
6. V. Yerokhov, I. Melnyk, A. Tsisaruk and I. Semochko, *Opto-electronics Review*, 2000, 8(4), 414.
7. T.-H. Chou, K.-Y. Cheng, T.-L. Chang, C.-J. Ting, H.-C. Hsu, C.-J. Wu, J.-H. Tsai, T.-Y. Huang, *Microelectronic Engineering*, 2009, 86, 628.
8. M.-L. Kuo, D. J. Poxson, Y. S. Kim, F. W. Mont, J. K. Kim, E. F. Schubert, and S.-Y. Lin, *Optics Letters*, 2008, 33(21), 2527.
9. C. G. Bernhard, *Endeavour*, 1967, 26, 79.
10. A. Gombert, W. Glaubitt, K. Rose, J. Dreibholz, B. Bläsi, A. Heinzl, D. Sporn, W. Döll and V. Wittwer, *Solar Energy*, 2000, 68(4), 357.
11. H. K. Raut, V. A. Ganesh, A. S. Nair, and S. Ramakrishna, *J. Mater. Chem.*, 2010, 20, 8134-8138.
12. J.-Q. Xi, M. F. Schubert, J. K. Kim, E. F. Schubert, M. Chen, S.-Y. Lin, W. Liu and J. A. Smart, *Nature Photon.* 2007, 1, 176.
13. S. L. Diedenhofen, G. Vecchi, R. E. Algra, A. Hartsuiker, O. L. Muskens, G. Immink, E. P. A. M. Bakkers, W. L. Vos, and J. G. Rivas, *Adv. Mater.* 2009, 21, 973.
14. J. Xiao. Y. Wu, W. Zhang, X. Bai, L. Yu, S. Li, G. Zhang, *Applied Surface Science*, 2008, 254, 5426.

15. H. Takato, M. Yamanaka, Y. Hayashi, R. Shimokawa, I. Hide, S. Gohda, F. Nagamine and H. Tsuboi, *Jpn. J. Appl. Phys.*, 1992, 31, L1665.
16. S. Chhajed, M. F. Schubert, J. K. Kim, and E. F. Schubert, *Appl. Phys. Lett.* 2008, 93, 251108.
17. Y.-F. Huang, S. Chattopadhyay, Y.-H. Jen, C.-Y. Peng, T.-A. Liu, Y.-K. Hsu, C.-L. Pan, H.-C. Lo, C.-H. Hsu, Y.-H. Chang, C.-S. Lee, K.-H. Chen and L.-C. Chen, *Nature Nanotech.* 2007, 2, 770.
18. H. Kobayashi, N. Moronuki and A. Kaneko, *International Journal of Precision Engineering and Manufacturing*, 2008, 9(1), 25.
19. T. Nakanishi, T. Hiraoka, A. Fujimoto, T. Okino, S. Sugimura, T. Shimada, K. Asakawa, *Japanese Journal of Applied Physics*, 2010, 49, 075001.
20. W.-L. Min, B. Jiang, and P. Jiang, *Adv. Mater.*, 2008, 20, 3914.
21. Y. Li, J. Zhang, S. Zhu, H. Dong, F. Jia, Z. Wang, Z. Sun, L. Zhang, Y. Li, H. Li, W. Xu, and B. Yang, *Adv. Mater.*, 2009, 21, 1.
22. Q. Chen, G. Hubbard, P. A. Shields, C. Liu, D. W. E. Allsopp, W. N. Wang, and S. Abbott, *Appl. Phys. Lett.*, 2009, 94, 263118.
23. J. Y. Chen and K. W. Sun, *Thin Solid Films*, 2011, 519, 5194.
24. K. Tadanaga, N. Yamaguchi, Y. Uraoka, A. Matsuda, T. Minami, M. Tatsumisago, *Thin Solid Films*, 2008, 516, 4526.
25. Y.-C. Chao, C.-Y. Chen, C.-A. Lin, Y.-A. Dai and J.-H. He, *J. Mater. Chem.*, 2010, 20, 8134.
26. Y. Liu, A. Das, S. Xu, Z. Lin, C. Xu, Z. L. Wang, A. Rohatgi, and C. P. Wong, *Adv. Energy Mater.* 2012, 2, 47.
27. Y.-J. Lee, D. S. Ruby, D. W. Peters, B. B. McKenzie, and J. W. P. Hsu, *Nano Lett.* 2008, 8(5), 1501.
28. H. Nakamura, Y. Yamaguchi, M. Miyazaki, H. Maeda, M. Uehara and P. Mulvaney, *Chem. Commun.*, 2002, 2844-2845.
29. E. M. Chan, R. A. Mathies and A. P. Alivisatos, *Nano. Lett.* 2003, 3(2), 199.

30. X. Z. Lin, A. D. Terepka, and H. Yang, *Nano. Lett.* 2004, 4(11), 2227.
31. S. A. Khan, A. Günther, M. A. Schmidt, and K. F. Jensen, *Langmuir*, 2004, 20, 8604.
32. E. M. Chan, A. P. Alivisatos, and R. A. Mathies, *J. Am. Chem. Soc.*, 2005, 127, 13854.
33. S. H. Lee, H. J. Lee, D. Oh, S. W. Lee, H. Goto, R. Buchmaster, T. Yasukawa, T. Matsue, S.-K. Hong, H. Ko, M.-W. Cho, and T. Yao, *J. Phys. Chem. B*, 2006, 110(9), 3856.
34. S. A. Khan and K. F. Jensen, *Adv. Mater.* 2007, 19, 2556.
35. Kevin M. McPeak and Jason B. Baxter, *Cryst. Growth Des.*, 2009, 9 (10), pp 4538–4545
36. P.-H. Mugdur, Y.-J. Chang, S.-Y. Han, A.A. Morrone, S.-O. Ryu, T.J. Lee, C.-H. Chang, *J. Electrochem. Soc.*, 2007, 154(9), D482.
37. J. Y. Jung, N.-K. Park, S.-Y. Han, T. J. Lee, S. O. Ryu, C.-H. Chang, *Current Applied Physics*, 2008, 8, 720.
38. J.-S. Huang, C.-Y. Chou, C.-F. Lin, *Sol. Eng. Mater. Sol. Cells* 2009, 93, 1608..
39. Q. Li, V. Kumar, Y. Li, H. Zhang, T. J. Marks, and R. P. H. Chang, *Chem. Mater.* 2005, 17, 1001.
40. Z. Liu, J. Ya, L. E, *J. Solid State Electrochem.*, 2010, 14, 957.
41. Z. Zhang, S. J. Wang, T. Yu and T. Wu, *J. Phys. Chem. C*, 2007, 111, 17500.
42. A. Zainelabdin, S. Zaman, G. Amin, O. Nur, and M. Willander, *Crys. Growth Des.*, 2010, 10, 3250.
43. F. -W. Yuan, H. -J. Yang and H. -Y. Tuan, *J. Mater. Chem.*, 2011, 21, 13793.
44. S. -H. Yang, P. -C. Chen, S. -Y. Hong, *Current Applied Physics*, 2009, 9, e180.
45. G. -N. He, B. Huang, H. Shen, *J. Cryst. Growth.*, 2010, 312, 3619.
46. B. C. Bunker, P. C. Rieke, B. J. Tarasevich, A. A. Campbell, G. E. Fryxell, G. L. Graff, L. Song, J. Liu, J. W. Virden, G. L. McVay, *Science*, 1994, 264, 48.
47. T.-L. Sounart, J. Liu, J.A. Voigt, M. Huo, E.D. Spoeke, B. McKenzie, *J. Am. Chem. Soc.* 2007, 129, 15786.

48. K.M. McPeak, T.P. Le, N.G. britton, Z.S. Nickolov, Y.A. Elabd, J.B. Baxter, *Langmuir*, 2011, 27, 3672..
49. Y.-J. Lee, T.L. Sounart, J. Liu, E.D. Spoerke, B.B. McKenzie, J.W.P. Hsu, J.A. Voigt, *Cryst. Growth & Design*, 2008, 8, 2036.
50. K. Govender, D.S. Boyle, P.B. Kenway, P.O'Brien, *J. Mater. Chem.*, 2004, 14, 2575.
51. M. Kokotov, G. Hodes, *Chem. Mater.* 2008, 20, 4542.
52. G. He, B. Huang, H. Shen, *J. Cryst. Growth.* 2010, 312, 3619.
53. J. Zhang, Y. Li, X. Zhang, and B. Yang, *Adv. Mater.*, 2010, 22, 4249.



Scheme 1. A schematic diagram of microreactor-assisted nanomaterial deposition (MANDTM) process and concept.

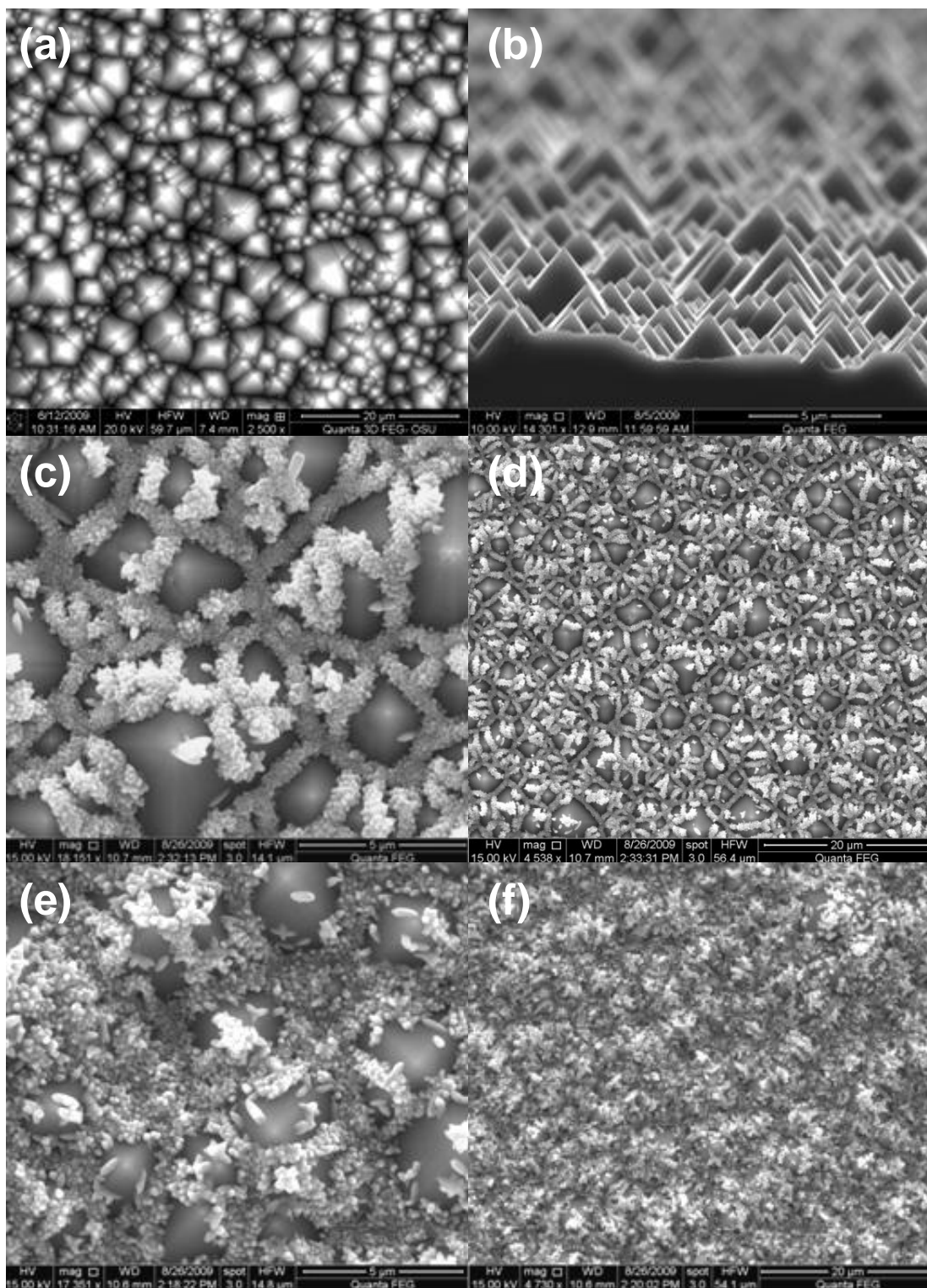


Figure 1. SEM images of (a) top view and (b) tilted cross section of textured silicon, top view of nanostructured ZnO deposition (c), (d) without seed layer, and (e), (f) with seed layer prepared by Zn(Ac)+Ammonium(Ac): (b),(C), and (e) in 5 um scale bar, (a), (d), and (f) in 20 um scale bar.

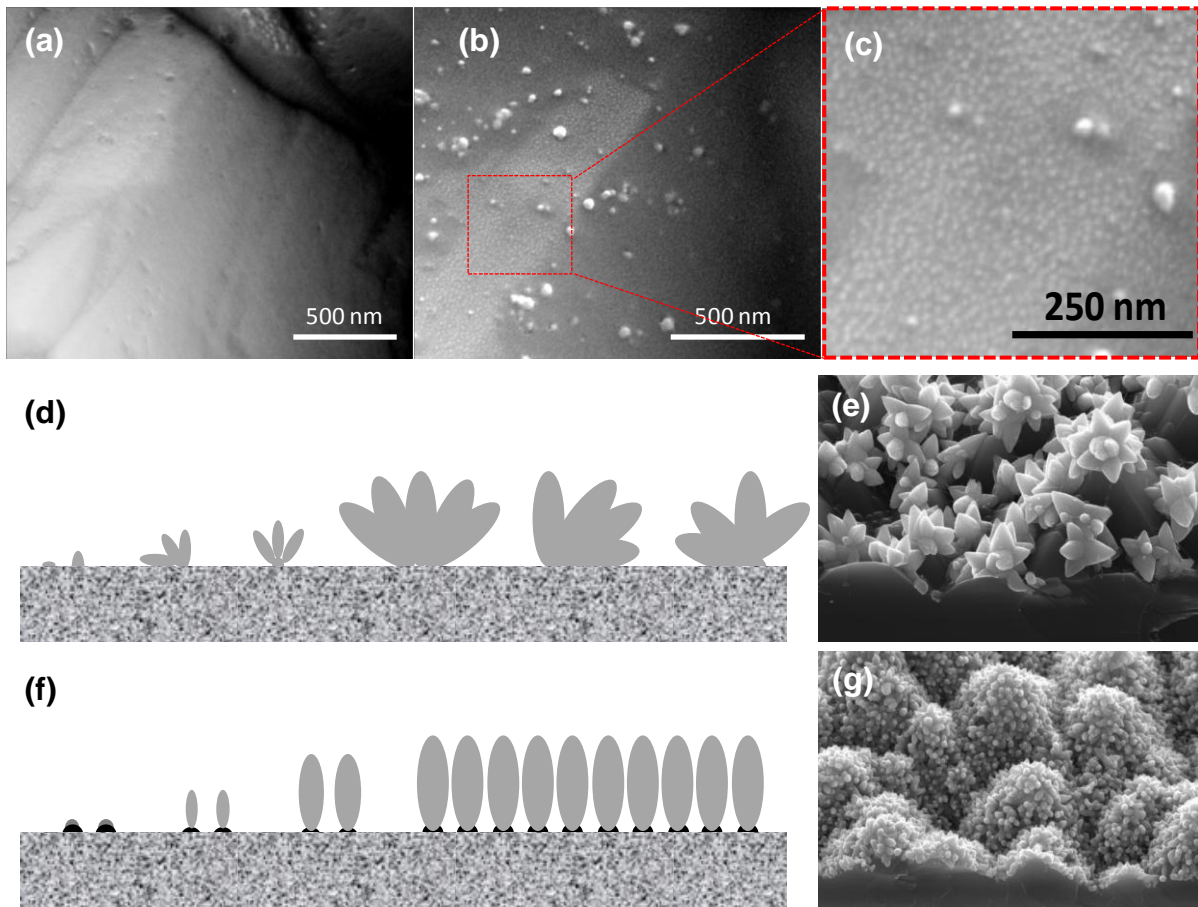


Figure 2. SEM images of (a) bare textured Silicon, (b) Ag seeded on textured silicon and (c) enlarge of (b), schematic diagrams of different nanostructured ZnO growths: (d, e) without Ag NPs seed layer and (f, g) with Ag NPs seed layer.

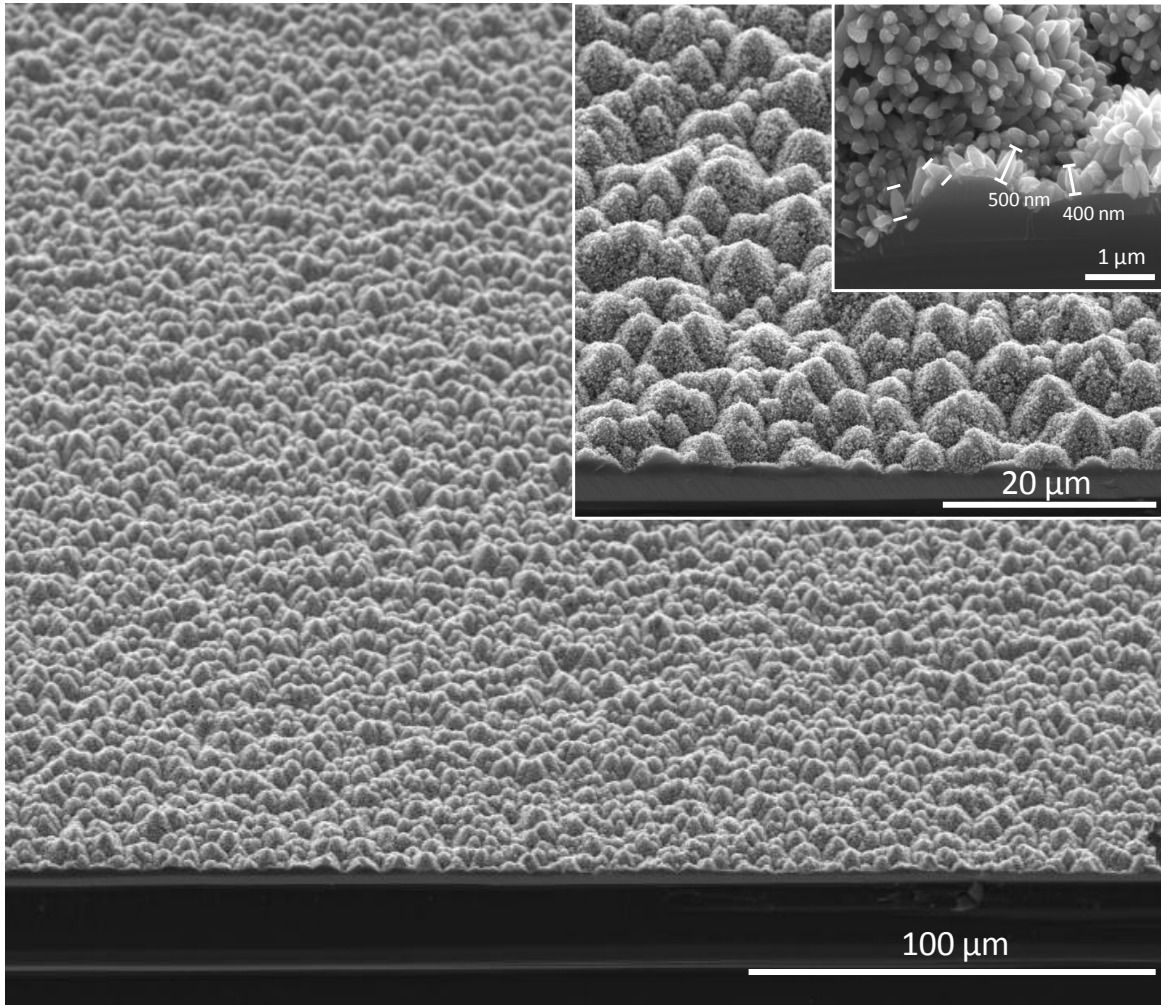


Figure 3. Tilted cross sectional SEM images of nanostructured ZnO grown on textured pyramidal surface of silicon substrate with various magnifications.

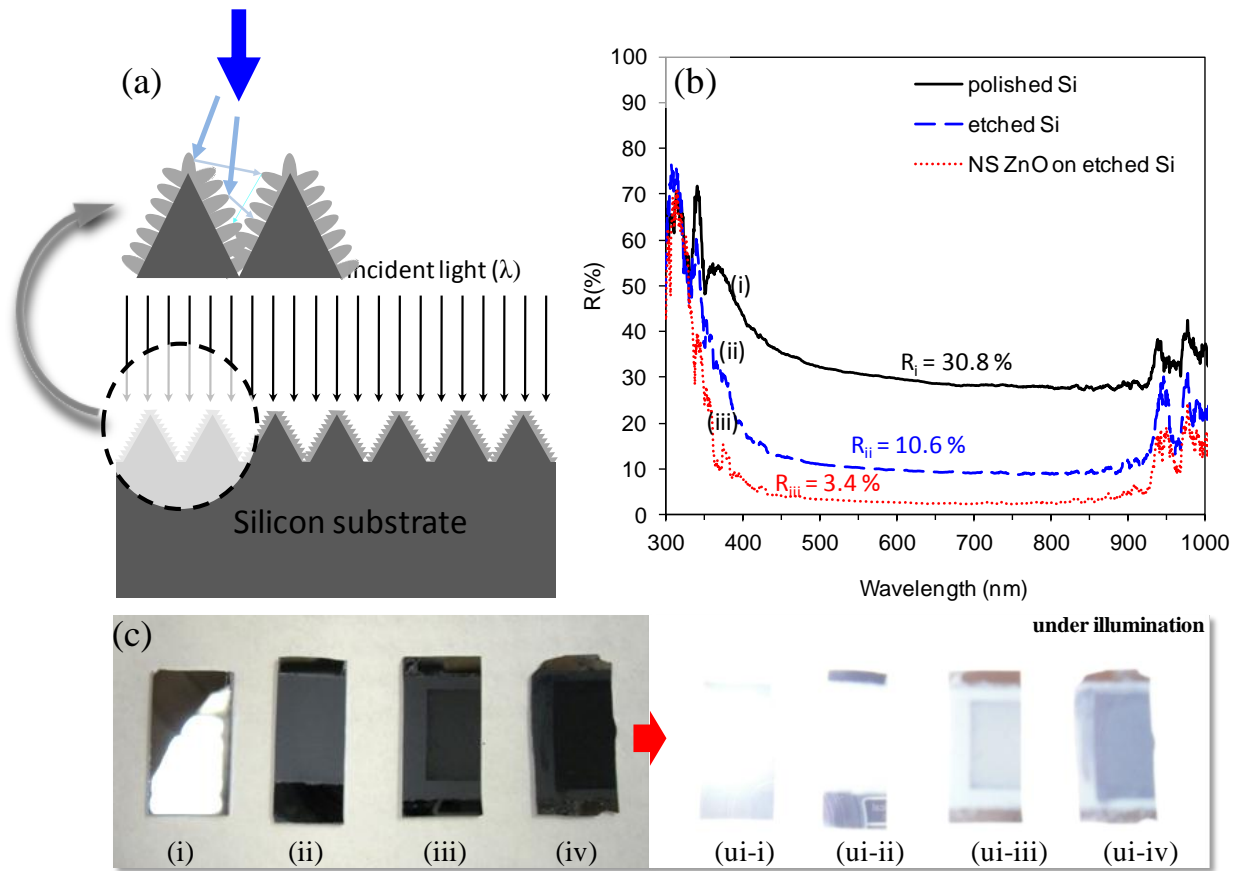


Figure 4. (a) A schematic diagram of light trapping in nanostructured ZnO on textured pyramidal surface of silicon substrate, (b) reflectance of polished silicon substrate (— black), textured silicon substrate (--- blue), and nanostructured ZnO grown (···· red) on textured silicon and (c) optical images of (i) polished silicon, (ii) textured surface silicon, (iii) ZnO deposition without seed layer on textured surface silicon, (iv) ZnO deposition with seed layer on textured surface silicon with/without illumination.

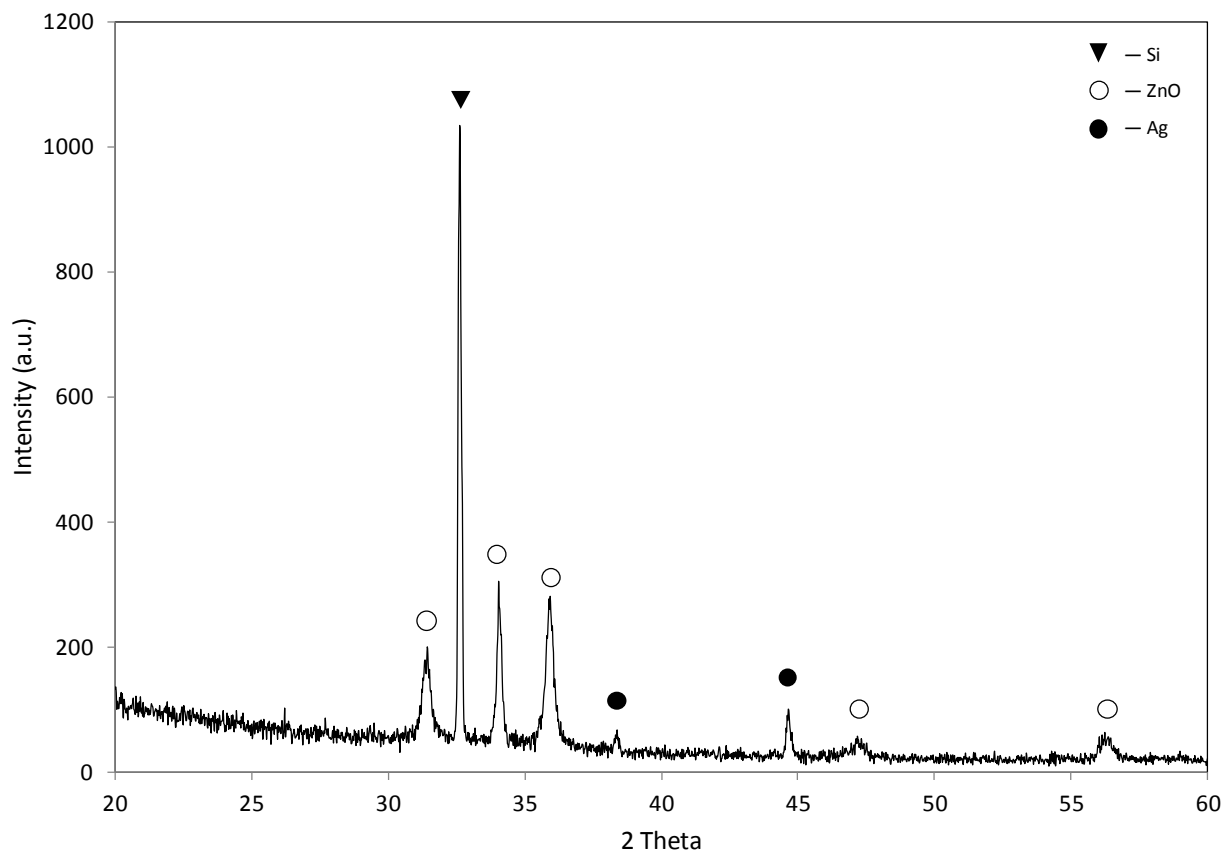
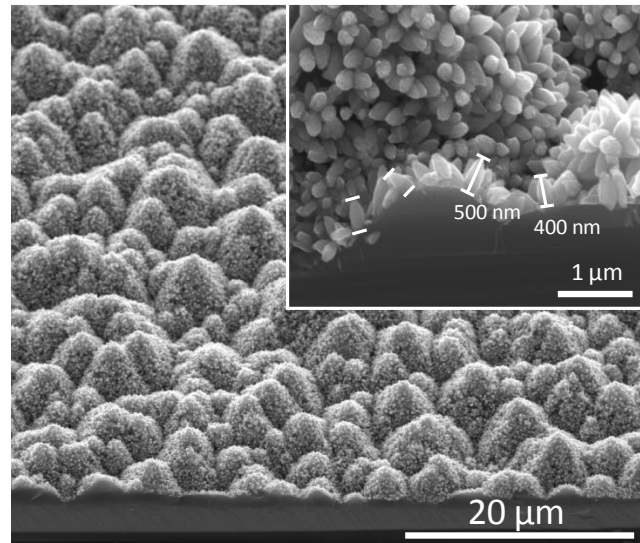
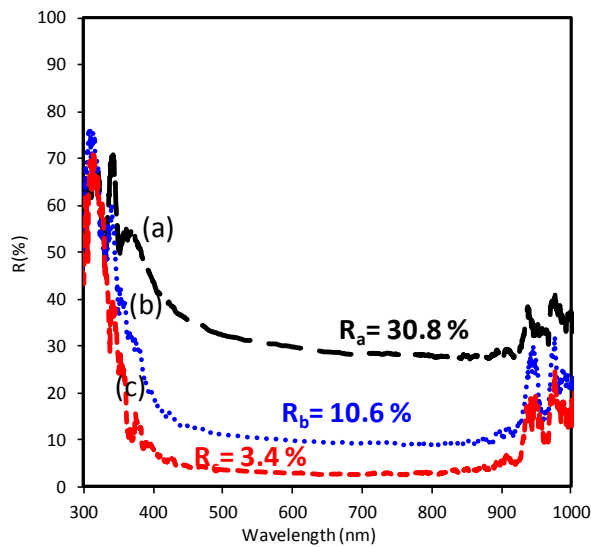


Figure 5. XRD spectra of nanostructured ZnO on textured Silicon (\blacktriangledown - silicon substrate, \circ - nanostructured ZnO, \bullet - Ag nanoparticles).

The table of contents entry

Nanostructured ZnO as Biomimetic Anti-reflective Coatings on Textured Silicon Using a Continuous Solution Process

Seung-Yeol Han,* Brian K. Paul and Chih-hung Chang*



Supplementary Information

Nanostructured ZnO as Biomimetic Anti-reflective Coatings on Textured Silicon Using a Continuous Solution Process

Seung-Yeol Han,^{a,*} Brian K. Paul^b and Chih-hung Chang^{a,*}

^a *School of Chemical, Biological, and Environmental Engineering, Oregon State University, 102
Gleeson Hall, Corvallis, OR, 97331, USA.*

^b *School of Mechanical, Industrial and Manufacturing Engineering, Oregon State University,
204 Rogers Hall, Corvallis, OR, 97331, USA.*

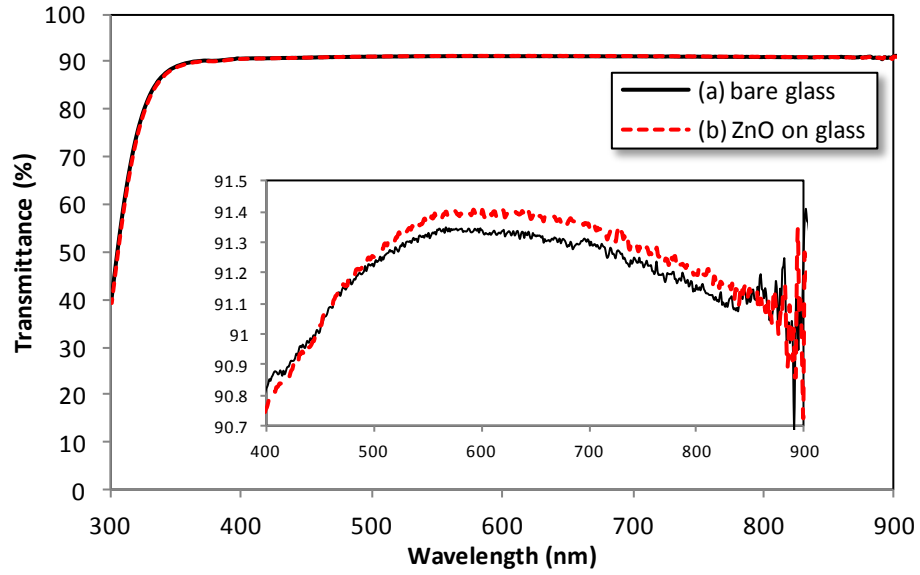


Figure S1. Transmittance of nanostructured ZnO deposition on glass substrate; (a) bare glass substrate and (b) nanostructured ZnO film on glass substrate.

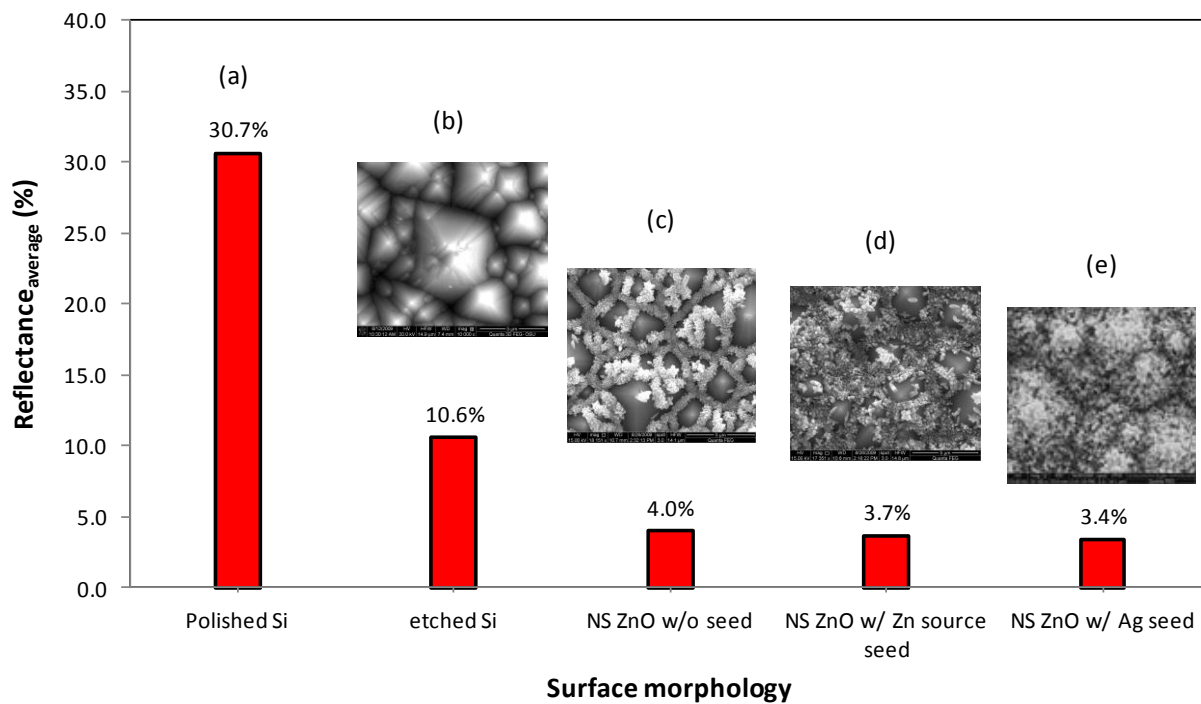


Figure S2. Averaged reflectance in the wavelength range of 400 ~ 900 nm over the AM1.5 solar photon spectra of various surface morphologies with top-view SEM images: (a) polished Si, (b) textured Si, (c) nanostructured (NS) ZnO without seed, (d) NS ZnO with Zn source seed and (e) NS ZnO with Ag nanoparticles seed.